Spectral Subband Centroid Energy Vectors Algorithm and Artificial Neural Networks for Acoustic Emission Pattern Classification

Marcus Tulius Barros FLORENTINO[1,2], Edson Guedes da COSTA[1],
Tarso Vilela FERREIRA[1,3], André Dantas GERMANO[1]
[1]*Post-graduation Program in Electrical Engineering (PPgEE/COPELE), Federal University of Campina Grande, Campina Grande, 58429-900, Brazil*
[2]*Federal University of Recôncavo da Bahia, Cruz das Almas, 44380-000, Brazil*
[3]*Post-graduation Program in Electrical Engineering (PROEE), Federal University of Sergipe, São Cristóvão, 49100-000, Brazil*
marcus.florentino@ee.ufcg.edu.br

***Abstract*—This work proposes and evaluates a methodology for monitoring and diagnosis of polymeric insulators in operation based on the parameterization of acoustic emissions (AE) created by corona and electrical surface discharges. The parameterization was performed with the use of the spectral subband centroid energy vectors (SSCEV) algorithm, which compresses the frequency spectrum and presents the results of the AE energies in several frequency bands. Thus, it was possible to calculate the dominant acoustic emission frequencies. This parameter was used as reference for an operating point of the insulators and, therefore, it was used to classify them. This classification was correlated to the classification obtained by visual inspection in the laboratory, where the insulators were divided into three distinct classes: clean, polluted and damaged. Aiming to insert an aid to the decision-making, this work still proposes the use of artificial neural networks (ANN) for pattern recognition. In this way, we performed a sensitivity analysis of the parameters that influence the SSCEV and ANN, in order to obtain the values and configurations with higher performance. The use of Levenberg-Marquardt training algorithm has proved to be more suitable, since it showed hit rates and convergence up to 97.66 percent and 70 epochs, respectively.**

***Index Terms*—acoustic emission, artificial neural networks, condition monitoring, corona, insulators.**

I. Introduction

The ability to anticipate, identify and diagnose a failure may be the critical difference between the shutdown and normal operation of a transmission line. The diagnosis should guide the decision-making process of the maintenance teams regarding the needs for repairs and replacements in-line components [1].

The monitoring and diagnosis of polymeric insulators in operation are not easy tasks. First, due to the numerous quantities of insulators in a transmission line and, secondly, due to the quantity and complexity of the physical parameters involved [1]. In this way, methods that help the monitoring and diagnosis of insulator processes are in ongoing development [2].

Periodic inspections are one of the safest and applicable ways of obtaining operational data from polymeric insulators. Some in-service inspection techniques combine non-invasive procedures with the possibility of gathering a significant amount of data to allow making estimations about insulators conditions. These estimations become consistent when performed with the use of intelligent systems capable of recognizing data patterns and classifying them adequately [3]. In several research fields, the use of intelligent classifier systems has been consolidated in the data and signal processing. Researchers have presented modeling solutions that have proven to be useful in many applications. The use of classifiers based on Fuzzy models is well documented in [4]. Approaches based on heuristic and hybrid models are presented in [5] and [6]. Discussions about a new artificial neural network training algorithm was proposed by [7].

Regarding the techniques for obtaining electrical insulators parameters, the usual inspection techniques are visual inspection, ultraviolet light detection, thermal, acoustic and electric field distribution measurements and hydrophobicity classification [1-2],[8-9].

Several researchers have successfully used acoustic and electromagnetic waves detection methods of corona and electrical surface discharges created by intense and local electric fields on insulator surfaces [3],[10]. Acoustic emission (AE) monitoring techniques present immunity to electromagnetic noise [11-12]. They are low cost and, furthermore, allow the splitting acoustic noises into distinct and limited ranges of the frequency spectrum and the application of pattern recognition algorithms [3]. In this way, signal analysis techniques based on Wavelet transform [13,14], Fourier transform [15,16], Artificial Neural Networks (ANN) and so on, have been used in order to characterize and classify the corona and electrical surface discharge signals [3],[11],[17-19].

One of those AE methods for monitoring insulators is based on the analysis of the acoustic noise emitted in the ultrasonic (US) range, then processed by the Spectral Subband Centroid Energy Vectors (SSCEV) algorithm [11],[19]. The SSCEV algorithm allows calculating the AE energy of discharges in the ultrasound range and its application has already been evaluated in the diagnosis of ceramic insulators [11].

This work was supported by CNPq and Proex/CAPES, which provided the scholarships.

Digital Object Identifier 10.4316/AECE.2019.03006

Several studies have shown the correlation between the operating conditions of the insulators, when corona and electrical surface discharges occur, and the emission of electromagnetic and acoustic waves [11-12],[20-23]. Normally, the energy of the AE is proportional to the intensity of the discharge to which it is associated, in the air. However, the frequency of the AE is inversely proportional to the energy released by the discharge [24-25]. During the occurrence of electric discharge in the air, a great amount of energy is concentrated in limited bands of frequency (called dominant frequencies) and this frequency depends on the nature of the discharge [25].

This work presents a methodology that uses the SSCEV algorithm to calculate the dominant acoustic emission frequency in order to correlate this parameter with the operating conditions of polymeric insulators. The operating conditions of the polymeric insulators used in this work were obtained through visual inspection in a laboratory and it was possible to separate them into three distinct operation classes: clean, polluted and damaged.

Therefore, the main contribution of this work is to provide a methodology for monitoring and diagnosis of polymeric insulators which is based on the analysis of the spectral behavior of the AE, by calculating the dominant acoustic emission frequency, and which supports the visual inspection.

In order to support the decision-making process, this work proposes the use of ANN to classify AE patterns. For this purpose, this paper presents the results of sensitivity analysis performed with the main variables of the SSCEV algorithm which influences the ANN configuration. In this way, the aim of this sensitivity analyzes is to highlight which parameters values best fit the proposed methodology and which configurations and algorithms of ANN training, between Resilient Propagation and Levenberg-Marquardt, presents better performance.

II. Dominant Acoustic Emission Frequency

The detection of AE from the corona and surface discharges is a viable alternative to methods that are sensitive to electromagnetic fields. US acoustic inspections are based on a mechanical effect of the electric discharges, possible because the corona and surface discharges that occur near the polluted and damaged polymeric insulators results in located and instantaneous energy release.

Furthermore, the noise coming from superficial discharges releases more energy in the ultrasonic band, especially when the discharges happen in the air [24]. Figure 1 shows the behavior of the mechanical energy from the electrical discharges in the different acoustic frequency bands [25]. For a greater amount of radiated energy, the frequency of dominant acoustic radiation is lower, as observed in the occurrence of ruptures. For the higher dominant frequencies, the radiated energy is lower, as occurs with the corona discharges.

According to the curve represented in Figure 1, the dominant frequency for different disruptive distances is expressed by (1):

$$f = c\sqrt{\frac{P}{W}} \tag{1}$$

where f is the dominant frequency in Hz, c is the velocity of air in m/s, P is the atmospheric pressure in Pa and W is the mechanical energy of the discharge in J/m [25].

The alternative way to calculate the dominant acoustic frequency proposed by this work and based on the extraction of the SSCEV will be shown in the material and methods section.

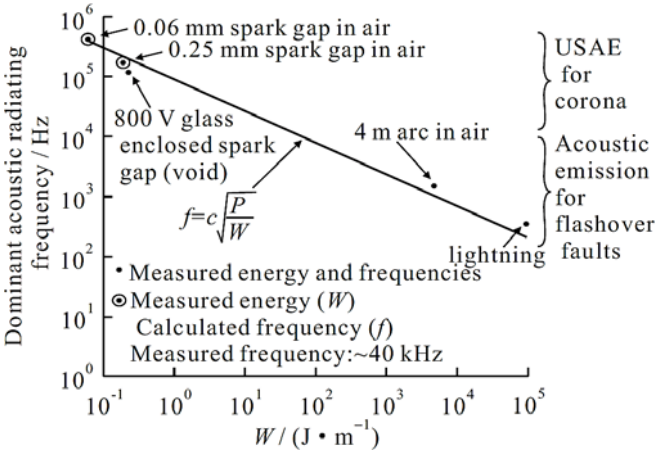

Figure 1. Acoustic emission radiating frequencies measured from lightning, long sparks and partial discharges versus discharge energy (energy per unit length, J/m) [adapted from [25]].

III. Spectral Subband Centroid Energy Vectors

The extraction of signal attributes is one of the most important tasks for the recognition of acoustic patterns. It requires the choice of an appropriate mathematical procedure, which highlights the most relevant information and, at the same time, discards redundant or irrelevant information.

Among several methods, there are those for the extraction of speech attributes, which can be based, for example, on cepstral coefficients and on the spectral subband centroids (SSC) [26]. Both methods present computational processes similar to each other; however, the use of SSC is a more advantageous alternative to cepstral coefficients because they allow the proper separation of the signal in the presence of unwanted noises [26-27].

The SSC processing is performed according to the parameters defined for the splitting of the signal frequency band, in a fixed amount of subbands, and by the calculation of the centroid in each of the subbands [27]. The parameters to be defined are:

- Numbers of filters for splitting the frequency spectrum;
- Filters' middle frequency and break frequency;
- Filters' format;
- Overlap percentage.

The SSCEV method is based on SSC processing and may be utilized for recognition and extraction of ultrasonic noise features considering the spectral centroid energies. This algorithm splits the frequency spectrum into a number of overlapping subbands, locates the centroids of each subband and calculates the energy in the proximity of each centroid.

The estimation procedures according to SSCEV algorithm are described below [11],[19]:

1. For each US signal recorded, the spectrum is calculated

through fast Fourier transform (FFT);

2. Then, the spectrum is divided into several subbands, through the application of rectangular superposed bandpass filters;
3. The centroid localization C_H for each subband is calculated by using (2):

$$C_H = \frac{\sum_{j=0}^{N-1} H_m(j) \cdot P(j)}{\sum_{j=0}^{N-1} P(j)}, \quad (2)$$

where P(j) is the estimated spectrum, $H_m(j)$ is the vector of frequencies, and N is the number of samples (subbands) limited by the filter;

4. The energy E_C associated with each centroid is calculated through (3):

$$E_C = \sum_{j=C_H-\delta \cdot N}^{C_H+\delta \cdot N} P(j), \quad (3)$$

where δ defines how wide the range in the neighborhood of the centroid is. The energy of the SSCEV element is then calculated within the range defined by δ.

IV. Material and Methods

A. Material

All the insulators used in the laboratory tests were taken from transmission lines. The tested insulators, nine units, had different levels of degradation and surface pollution.

In all tests, we used the same insulator model and manufacturer, for 230 kV class. A photograph and the dimensional schematic of the model of insulator used in this work, are shown in Figure 2(a) and Figure 2(b), respectively.

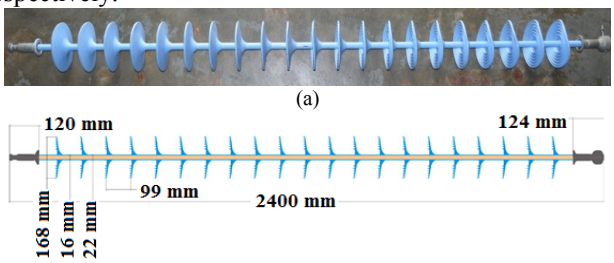

Figure 2. (a) 230 kV model of polymeric insulator photography and (b) dimensional characteristics of the polymeric insulator.

B. Visual Inspection

The flowchart of the methods applied in this work is shown in Figure 3. The experimental procedures started with the separation of insulators in operation classes by visual inspection. Thus, we analyzed the following physical conditions of the insulators: surface pollution, presence of erosion and tracking in the polymer coating, exposure of the rod, corrosion condition of the end fittings and the state of the connections between the core and end fittings.

The analysis of the insulators conditions allows us to distinct three groups with different degradation levels. The insulators 1, 2 and 3 comprise the Group 1, which were clean and presented no visual signs of degradation. Three other insulators comprise the Group 2 (insulators 4, 5 and 6) which contained surface pollution. Three other insulators (insulators 7, 8 and 9) comprise the Group 3. Insulator 7 contains tracking and erosion on the coating. Insulator 8 contains core exposure and moisture in the bonds and insulator 9 contains core exposure and corrosion on the end fittings. The classification of the nine insulators into three groups with distinct operation classes, obtained from the visual inspection, is shown in Table I.

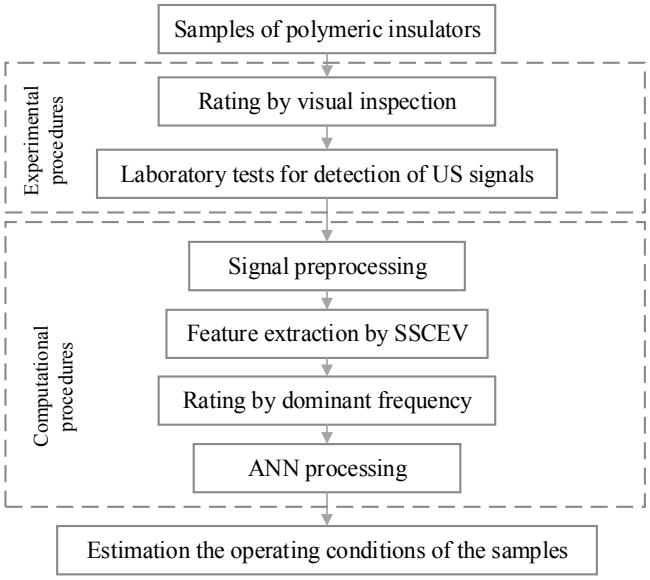

Figure 3. Flowchart of the methods.

TABLE I. GROUPS OF INSULATOR BY VISUAL INSPECTION

Group	Operation class	Insulators
1	Clean	01, 02 e 03
2	Polluted	04, 05 e 06
3	Damaged	07, 08 e 09

C. Laboratory Tests

The laboratory tests were performed under similar atmospheric conditions for all insulators and in a setup with geometrical characteristics that aimed to reproduce the conditions in a transmission line, as shown in Figure 4. The magnitude of the applied voltage was 132.8 kV, equivalent to the nominal voltage between the phase and the earth on the insulator.

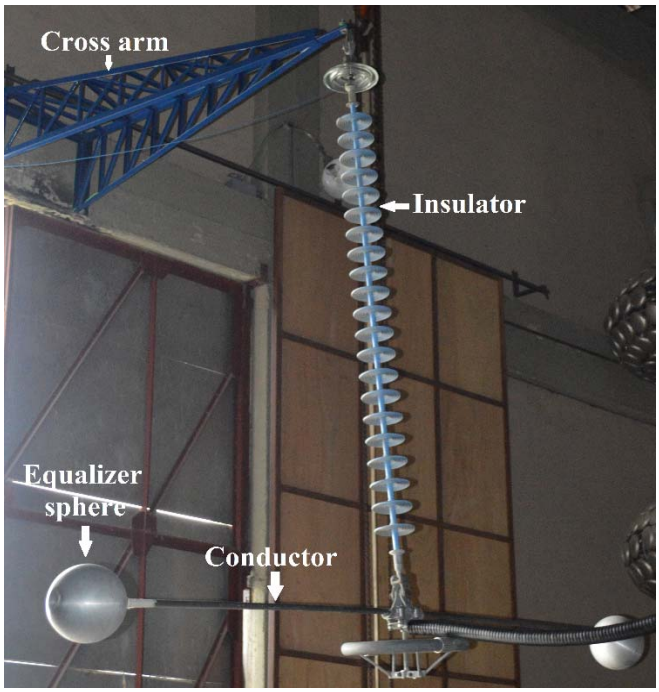

Figure 4. Photograph of the line condition emulation system.

In order to detect the ultrasonic noise signals, we used the

Ultrasonic 2000 MPH, equipped with the Trisonic Scanning Module, both manufactured by UE Systems. This setup detects the ultrasonic acoustic emitions and converts it to an audible frequency range (20 Hz < f < 3 kHz). Figure 5 shows the schematic of the voltage application and measuring system.

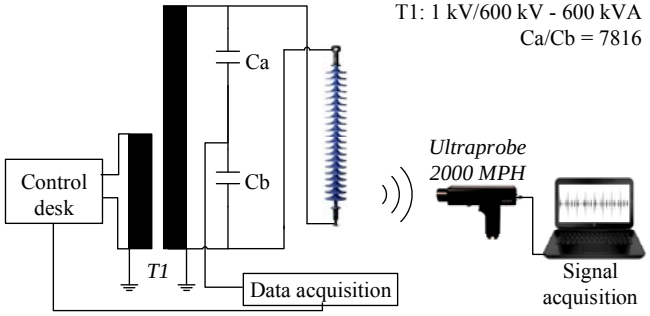

Figure 5. Diagram of the voltage application and measuring system.

About 15 minutes after the application of high voltage, the ultrasonic noises were recorded. The recordings were made in three different positions, 10 meters away from the insulator and with 120 degrees between them. In each position, the noises were recorded three times. Therefore, for each insulator we recorded nine audio samples. Each recorded audio samples has 30 seconds of duration. During laboratory tests, atmospheric conditions did not change significantly, maintaining a mean temperature, humidity and pressure standard, as shown in Table II.

TABLE II. ATMOSPHERIC CONDITIONS IN LABORATORY

Temperature (°C)	Humidity (%)	Atmospheric pressure (mbar)
26	70	955

D. Signal preprocessing

The signal preprocessing stage was developed with the purpose of creating a suitable database for the ANN. In this process, each 1.0 second (or a window of 60 industrial cycles, in Brazil) of each audio signal represented a sample for the ANN. Some overlapping in the windowing process was admitted (16.67%, 33.33 %, and 50 %; i.e. 10, 20 or 30 cycles of windowing steps), in order to increase the number of samples and reinforce the correlation between samples of the same class. Figure 6 shows the diagram that represents the windowing process.

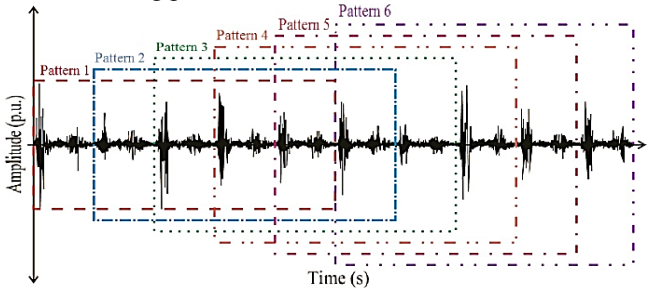

Figure 6. Diagram of windowing process.

E. Feature extraction by SSCEV

The result of the windowing process was the input of the SSCEV algorithm [11],[19]. In this step, as shown in Section II, several numbers of subbands (passband filters) were also tested (10, 20 or 30). In each one of three cases, overlap rates were compared between subbands: 10%, 25% and 50%.

F. Calculating the dominant frequency

The spectral behavior of the ultrasonic noise emitted by the insulators was evaluated according to the dominant acoustic radiating frequency [25]. The variable is closely related to the nature of electric discharge that occurs in insulator surface, as well as the energy emitted from the discharge [24].

The calculation of this parameter is used to classify the insulators within the operation classes presented in Table I and the result of this classification is compared to the one obtained by the visual inspection.

We calculate the dominant acoustic radiating frequency f (in kHz) by using (4):

$$f = \frac{\sum_{n=1}^{N} P(n) \cdot C_H^N}{\sum_{n=1}^{N} P(n)}, \quad (4)$$

where P(n) is the normalized power, n is the index that locates the normalized power in the corresponding centroid, C_H^N is the corresponding centroid, limited by the number of subbands, N is the number of subbands from SSCEV extraction.

G. ANN settings

The adaptive mathematical models based on the biological neuron were initially developed by [28]. ANNs are used for several purposes, including parameter classification and pattern recognition [29-30]. Thereby, ANNs are based on learning rules to establish their internal parameters, called synaptic weights. Among several network architectures that have been developed over decades, the multilayer perceptron (MLP), developed by [30], has gained prominence due to the simplicity, efficiency and reliability. By these reasons, we use MLP architecture in this work.

For training the ANN, we evaluate the use of two algorithms, the Resilient Propagation algorithm (RPROP), developed by [31], and the algorithm based on Levenberg-Marquardt (LM) [32]. The RPROP was chosen due to its advantages such as speed of convergence, reduced computational effort and good performance in the location of the minimum satisfactory error surface.

In addition, the Levenberg-Marquardt allows the acceleration of convergence during the backpropagation of the error [33]. The second derivative of the error function is taken into account, since the algorithm uses an approximation of Newton's method of optimization [32]. Equation (5) represents the Levenberg-Marquardt approximation:

$$\eta_{i+1}^{k} = \eta_{i}^{k} + [J^T J + \mu I]^{-1} J^T \xi \quad (5)$$

where η_i^k represents the neuron i of layer k, J is the Jacobian matrix representing the first derivatives of the error function in relation to the weights, ξ is the function error in the output of the network and I is the identity matrix.

The main characteristics of the Levenberg-Marquardt are:

- Convergence speed: the network converges in a few times. Experience shows that this quantity is around 70 epochs;
- Robustness: this makes it a very widespread algorithm, since the hit rates are high for solving

many problems;

- High computational effort: the price paid for its efficiency is the time elapsed in each training epoch;
- Limited efficiency for networks with up to a few hundred connections.

The accuracy rates as well as the number of training epochs and the processing time were taken as indicators of network performance. Each processing took place in 10 consecutive runs to obtain the average values of these parameters.

As a preliminary result and for use in the sensitivity analysis of the ANN processing, we found the relations between the number of neurons in the input layer (number of subbands used in SSCEV processing) and the number of neurons in the hidden layer. After several tests in the RPROP training, we found that the number of neurons in the hidden layer that allowed better performance was 1.5 neurons for each neuron in the input layer, resulting in 30, 60 and 90 neurons in the hidden layer. This same ratio between input layer and hidden layer neurons was not obtained in the Levenberg-Marquardt training, since there was no convergence. We search for the closest possible proportion to become comparable to the RPROP process, which allow convergence and high performance, and we found the ratio of 0.9 neurons in the hidden layer to each neuron in the input layer in the Levenberg-Marquardt training, resulting in 18, 36 and 54 neurons in the hidden layer.

In all cases, the number of neurons in the output layer is equal to three, which corresponds to the number of operation classes of the insulators (three groups with different degradation levels).

The dataset of the work is available on the link below: http://bit.do/paperAECE-6792.

H. ANN Architecture for Sensitivity Analysis

All possibilities of settings variations were considered, generating several sets of databases during the stages of preprocessing of the signals and attribute extraction. An amount of 27 cases was obtained, which are compared according to the parameters summarized in Table III. Each one of the 27 cases fed the ANN processing. In order to train the ANN in a depolarized way, each class must contain the same number of samples. This last premise was obeyed when we distinguished the classes of the insulators, as presented in Table I.

TABLE III. VARIATION OF PARAMETERS FOR SENSITIVITY ANALYSIS

Step	Parameter	Quantity
Preprocessing of signals	Windowing steps (cycles) Time superposition rate (%)	10, 20 or 30 83, 67 or 50
Feature extraction by SSCEV	Subbands Superposition rate (%)	10, 20 or 30 10, 25 or 50
ANN processing	Input layer neurons Hidden layer neurons in RPROP Hidden layer neurons in Levenberg-Marquardt	20, 40 or 60 30, 60 or 90 18, 36 or 54

V. RESULTS AND DISCUSSION

A. Feature Extraction by SSCEV

The complexity of the proposed task, which is the classification of spectral patterns, is illustratively exemplified in Figures 7, 9 and 11, where all of the SSCEV are plotted, for each group, in a superposed manner. It is not so clear in Figures 7, 9 and 11 that there are specific regions of the graphics that are exclusive of a determined class, making the distinction difficult. For a clearer visualization of the spectral regions of interest, Figures 8, 10 and 12 presents the mean values for each class.

The graphs shown in Figures 7, 9 and 11 were constructed from the preprocessing of the ultrasonic noise signals, as presented in section IV-D, and extraction of attributes according to the SSCEV method.

Each of the graphs seen in Figures 7, 9 and 11 present 4725 curves, each one corresponding to a SSCEV. Since 3 insulators are shown in each graphic, we have 1575 vectors representing the spectral behavior of each insulator. This amount of vector patterns was obtained in the windowing stage, with a superposition rate of 83%, which was the maximum used in this work, as presented in Table III. The number of subbands used in the processing of SSCEV for energy calculation, associated with the overlapping rate between subbands, indicates the degree of spectral detail. Therefore, for illustration purpose, we only present the graphical results for a number of 1575 standards per insulator, with 30 subbands splitting the spectrum and overlapping by 50%.

The class that represents the Group 1 with cleaned insulators was analyzed. Figure 7 shows the results of SSCEV for insulators 01, 02, and 03. Figure 8 shows the mean values of the results shown in Figure 7. The dominant frequency, obtained from (4), found for insulator 01 was 2.33 kHz. This result is exactly the frequency which concentrates most of the energy of SSCEV. Applying the same rule, the dominant frequency found for insulator 02 was 2.32 kHz, and for insulator 03 was 2.31 kHz.

According to [25], the discharge energy is inversely proportional to the frequency of the acoustic radiation. Therefore, the higher the frequency, the lower the emitted energy and, consequently, the lower the discharge or the harmful potential on the insulator. Thus, among the three, the insulator 01, with the highest dominant frequency, performed best in this class.

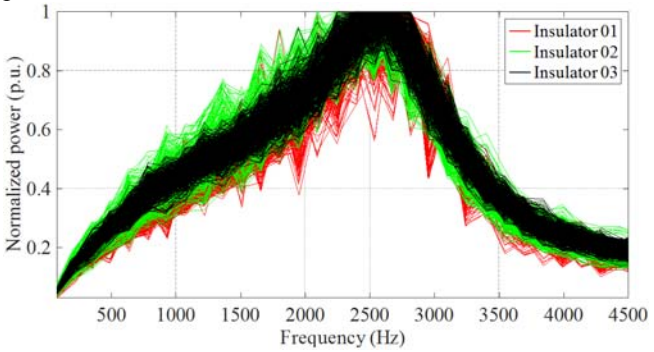

Figure 7. Superposed plot of 1575 samples SSCEV obtained from each one of the insulators 01, 02 and 03.

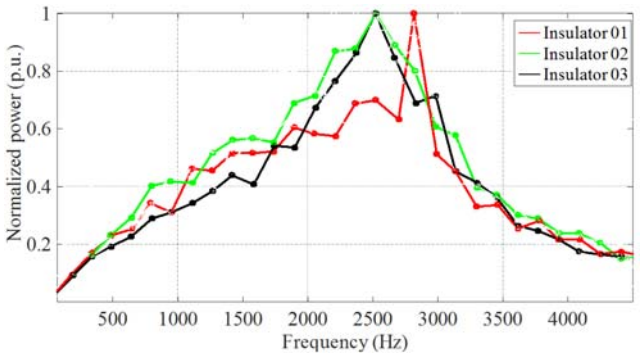

Figure 8. Mean values of SSCEV obtained from insulators 01, 02 and 03.

Insulators 04, 05 and 06 composed the group of insulators containing pollution deposited on the surface. This group, however, did not have characteristics of physical degradation. Figure 9 shows the results of SSCEV for insulators 04, 05 and 06. Figure 10 shows the mean values of the results shown in Figure 9. The dominant frequency found for the insulator 04 was 2.30 kHz, whereas in insulator 05 was 2.13 kHz, and the insulator 06 was 2.19 kHz.

Figure 11 shows the results of SSCEV for the insulators 07, 08 and 09, which composed the group of damaged insulators. Figure 12 shows the mean values of the results shown in Figure 11. The results for dominant frequency (calculated by (4)) for insulator 07 was 2.17 kHz, for insulator 08 was 2.25 kHz for insulator 09 was 2.25 kHz.

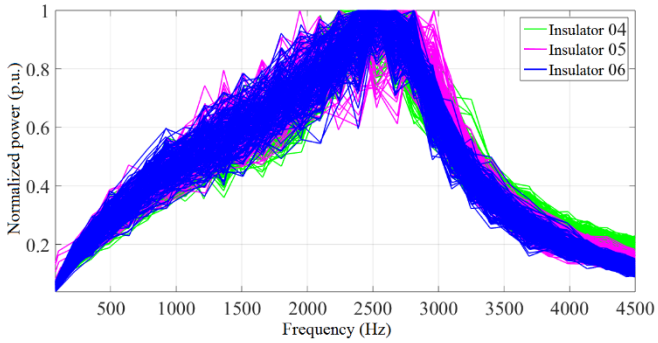

Figure 9. Superposed plot of 1575 samples SSCEV obtained from each one of the insulators 04, 05 and 06.

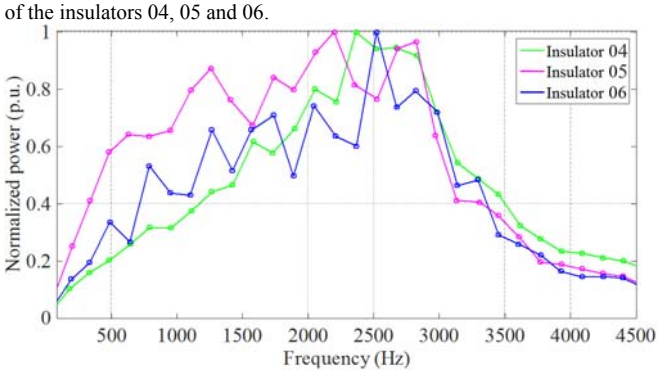

Figure 10. Mean values of SSCEV obtained from insulators 04, 05 and 06.

B. *Calculating the dominant frequency*

The dominant acoustic radiating frequencies obtained with ultrasonic noise samples for each insulator are shown in Table IV. We compared these results with the classification obtained from the visual inspection, according Table I.

The values shown in Table IV were used for classification of insulators by the spectral behavior. As shown in Table IV, we relocated some insulators in new operation classes, according to the intervals set out in Table V. We have chosen these intervals according to the results obtained for all nine insulators and we took into account two facts. First, we are dealing with the same physical phenomenon for all insulators, so the frequencies are very similar to each other and cause the thresholds to be very close between the different classes and, secondly, that the classes must represent the same amount of samples, in order to make the classification depolarized in computational processes.

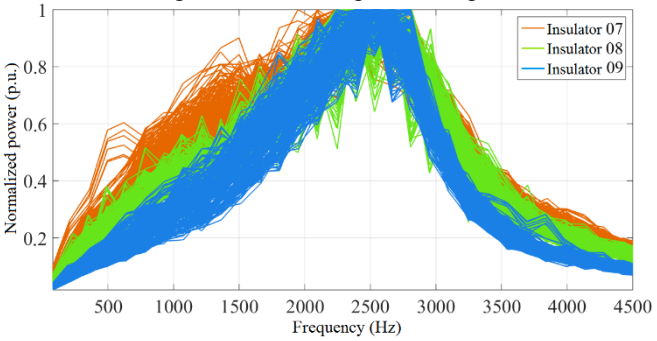

Figure 11. Superposed plot of 1575 samples SSCEV obtained from each one of the insulators 07, 08 and 09.

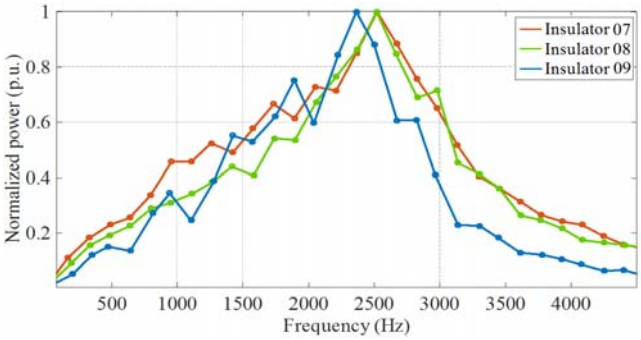

Figure 12. Mean values of SSCEV obtained from insulators 07, 08 and 09.

TABLE IV. CLASSIFICATION BY DOMINANT FREQUENCY

Operation class	Visual inspection	Classification by spectral behavior	
		Insulator	Dominant Frequency (kHz)
Clean	01, 02 and 03	01	2.33
		02	2.32
		03	2.31
Polluted	04, 05 and 06	04	2.30
		08	2.25
		09	2.25
Damaged	07, 08 and 09	06	2.19
		07	2.17
		05	2.13

TABLE V. INTERVAL FOR DOMINANT FREQUENCY

Group	Operation class	Dominant acoustic radiating frequency (kHz)
1	Clean	$f > 2.30$
2	Polluted	$2.20 < f \leq 2.30$
3	Damaged	$f \leq 2.20$

In this way, we can compare the classifications obtained by the different methods. Between the classification by the visual inspection and the spectral behavior, there were differences for the insulators 05, 06, 08 and 09. The insulators 05 and 06 showed frequencies below the threshold for class 2 of polluted insulators and were reclassified to class 3 of damaged insulators. The insulators 08 and 09 presented frequencies above the threshold for class 3 of degraded insulators and were reclassified to class

2 of polluted insulators. The ratings were similar for the other insulators.

C. ANN Processing

The configurations of the vector patterns used in the SSCEV processing and the correspondent ANN configurations were presented in Table III, which serves for our sensitivity analysis. The data obtained for the whole group of insulators, differentiated by the three classes, served as input for the 27 configurations presented in Table III.

Furthermore, the ANN training was carried out with the input patterns configured according to the classification by the spectral behavior. Therefore, the following results were achieved based on the new classification obtained by calculating the dominant acoustic radiating frequency.

The 27 cases were evaluated and their results will be analyzed below. Figure 13 shows the results for the success rates obtained during ANN processing for all cases considered, using both RPROP, in blue, and Levenberg-Marquardt, in red. Figure 14 shows the average number of epochs used by each network configuration adopted, among 27 cases, taking into account the two learning algorithms: RPROP and Levenberg-Marquardt.

The success rates and the average number of epochs were obtained after 10 executions. As shown in Figure 13, the standard deviation values were low in all cases, indicating that the number of iterations was sufficient to characterize the results of ANN. Considering the average success rates of all cases, the best case obtained in RPROP processing was 88.37% and in the Levenberg-Marquardt processing was 97.66%.

As we can see in the behavior of the curves shown in Figure 13, the increase of subbands and, consequently, the increase of neurons in the input layer, it makes the network more effective, although its efficiency decreases with increasing number of epochs to achieve the result, as shown in Figure 14.

Therefore, a larger number of subbands, obtained in the SSCEV processing, makes the energy vectors more representative for pattern recognition, as the information is presented to the network in more detail.

This can be better analyzed if we compare the results for each number of input patterns, 1575, 792 and 531, as highlighted in the frames in Figure 13. The behavior of the curves is the same: for the same amount of patterns the increment of processing units allows the network to obtain better results. However, when we observe the behavior of lines 1 and 2, which represents the rate of decay of success rates, we note that the decrease of the number of patterns, although not changing the other parameters of the network, decreases in a more noticeable way the effectiveness of Levenberg-Marquardt algorithm in comparison to RPROP algorithm.

In Figure 14, the much faster convergence of the Levenberg-Marquardt algorithm is remarkable. While the RPROP converged between 200 and 700 times in all its cases, the Levenberg-Marquardt algorithm converged in a maximum of 70 epochs. This is justified by the approximation with Newton's method of optimization, which converges rapidly to the minimum error [32].

As an additional result, after evaluation between hyperbolic tangent and sigmoid function, the activation function that we choose to use in RPROP training was hyperbolic tangent. This function was chosen because of Image Set [-1, 1], which allows the network spread negative values, providing a more equalized training through the layers [34]. For Levenberg-Marquardt training, we used the sigmoid activation function. This choice was based on the number of tests in which the network reached the maximum number of epochs used: 100.

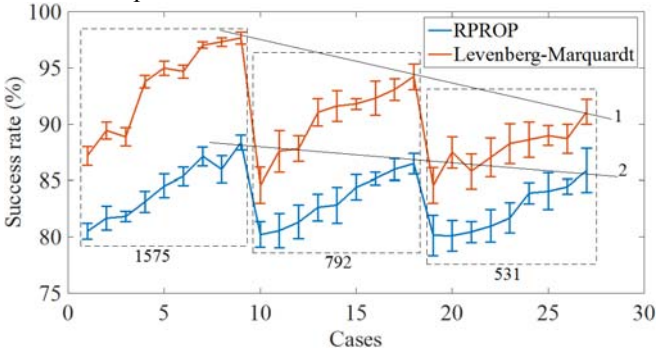

Figure 13. Average success rate (in %) for Resilient Propagation (RPROP) and Levenberg-Marquardt processings.

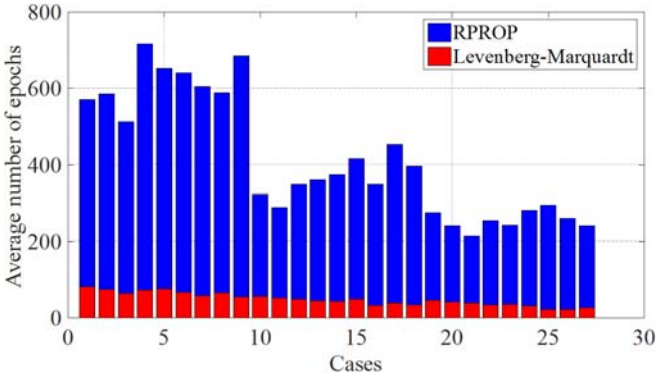

Figure 14. Average number of epochs for Resilient Propagation (RPROP) and Levenberg-Marquardt processings.

VI. Conclusion

In this paper, a methodology for monitoring and diagnosing the operating conditions of polymeric insulators based on acoustic emission parameters of the corona and surface discharges was evaluated. The parameter used to classify the insulators within the classes determined by visual inspection was the dominant acoustic emission frequency, where different values were obtained for this parameter among the different operating conditions of the insulators.

When analyzing the classification of the insulators, it is verified that the clean insulators had a dominant frequency higher than 2.30 kHz, whereas the insulators classified as polluted or damaged had dominant frequencies lower than 2.30 kHz, mostly more specifically in the range of 2.13 kHz to 2.25 kHz. These results show a close proximity of values that is justified, since we are analyzing the same phenomenon of electric discharge in different insulators, under similar atmospheric conditions, but with different physical and structural conditions. Therefore, the threshold for observing defects in insulators, for classification purposes, makes it necessary to use estimation methods to support decision-making.

The sensitivity analysis performed by the variation of the

main parameters of the SSCEV and, consequently, of the ANN, showed that the configurations that presented better performance (higher hit rates and low computational effort) were those that used larger amounts of signal samples (1575 patterns), subbands (30) and overlapping rate (50%) among subbands. It is remarkable that case 9 presented the best performance. This is noticeable both in the ANN training performed with the RPROP and the Levenberg-Marquardt algorithm, but the use of the Levenberg-Marquardt proved to be remarkably more suitable because it presented higher hit rates (up to 97.66%) and convergence up to 70 epochs.

Considering the above, this methodology is promising if we recognize it as an alternative to support visual inspection improvements, considering the correlations found in both classifications.

ACKNOWLEDGMENTS

The authors of this paper wish to demonstrate their gratitude to Eletrobras-Chesf, for the kindness to give their samples insulators, and CNPq and Proex/CAPES, which provided the scholarships.

REFERENCES

[1] Gubanski, S. M. Dernfalk, A.; Andersson J.; Hillborg, H. “Diagnostic Methods for Outdoor Polymeric Insulators.” IEEE Trans. Dielectrics and Electrical Insulation, vol. 14, n. 5, pp. 1065-1080, 2007. doi:10.1109/TDEI.2007.4339466

[2] Cigré Working Group B2.21, “Assessment of in-service Composite Insulators by using Diagnostic Tools.”, Electra, vol. 269, pp. 29-31, 2013.

[3] Al-Geelani, N. A.; Piah, M. A. M.; Bashir, N. “A Review on Hybrid Wavelet Regrouping Particle Swarm Optimization Neural Networks for Characterization of Partial Discharge Acoustic Signals.” Renewable and Sustainable Energy Reviews, vol. 45, pp. 20-35, 2015. doi:10.1016/j-rser.2015.01.047

[4] Herrera-Viedma, E.; López-Herrera, A. G. “A Review on Information Accessing Systems Based on Fuzzy Linguistic Modelling,” Int. Journal of Computational Intelligence Systems, vol. 3, n. 4, pp. 420-437, 2010. doi:10.1080/18756891.2010.9727711

[5] Pozna, C.; Precup, R.; Tar, J. K.; Škrjanc, I.; Preitl, S. "New results in modelling derived from Bayesian filtering," Knowledge-Based Systems, vol. 23, n. 2, 2010, pp. 182-194. doi:10.1016/j.knosys.2009.11.015

[6] Takács, A.; Kovács, L.; Rudas, I. J.; Precup, R.; Haidegger, T. "Models for Force Control in Telesurgical Robot Systems," Acta Polytechnica Hungarica, vol. 12, n. 8, 2015, pp. 95-114. doi:10.12700/APH.12.8.2015.8.6

[7] Ruiz-Rangel, J.; Hernandez, C. J. A.; Gonzalez, L. M.; Molinares, D. J. "ERNEAD: Training of Artificial Neural Networks Based on a Genetic Algorithm and Finite Automata Theory," Int. Journal of Artificial Intelligence, vol. 16, n. 1, 2018, pp 214-253. doi:http://hdl.handle.net/20.500.12442/1863

[8] Gorur, R. S.; Cherney, E. A.; Burnham, J. T. Outdoor insulators, 1st ed. Phoenix: Ravi S. Gorur Inc., 1999.

[9] Vosloo, W. L.; Macey, R. E.; Tourreil, C. The Practical Guide to High Voltage Insulators. South Africa: Crown Publications cc, vol. 3, pp. 220, 2006.

[10] Ramirez, C.; Moore, P. J. “Identification of surface discharges over new and aged polymeric chain insulators using a non invasive method”, In: IEEE Proc. 41st Int. Universities Power Eng. Conf., 2006. pp. 903–906. doi:10.1109/UPEC.2006.367610

[11] Ferreira, T. V.; Germano, A. D.; Costa, E. G. “Ultrasound and Artificial Intelligence Applied to the Pollution Estimation in Insulations.” IEEE Trans. Power Delivery, vol. 12, pp. 583-589, 2012. doi:10.1109/TPWRD.2011.2178042

[12] Menon. R.; Kolambekar, S.; Buch, N. J.; Ramamoorty, M. “Correlation of acoustic emission method and electrical method for detection of partial discharges in transformers,” in Proc. IEEE 7th Int. Conf. Solid Dielectrics, pp. 299-302, Jun. 2001. doi:10.1109/ICSD.2001.955631

[13] Muniraj, C.; Chandrasekar, S. “Condition Monitoring of Outdoor Polymeric Insulators Using Wavelets and ANFIS”, In: IEEE Int. Conf. on Power and Energy, Kuala Lumpur, 2010, pp. 346-351. doi:10.1109/PECON.2010.5697607

[14] Nyamupangedengu, C.; Luhlanga, L. P.; Letlape T. “Acoustic and HF Detection of Defects on Porcelain Pin Insulators”, In: IEEE Power Eng. Society Conf. and Expo. in Africa, Johannesburg, 2007. doi:10.1109/PESAFR.2007.4498111

[15] Shurrab, I. Y.; El-Hag, A.; Assaleh, K.; Ghunem, R. “Partial Discharge On-Line Monitoring of Outdoor Insulators”, In: IEEE Int. Symp. on Electrical Insulation, San Juan, 2012, pp. 391-394. doi:10.1109/ELINSL.2012.6251496

[16] Gorur, R. S.; Chang, J. W.; Amburgey, O. G. "Surface hydrophobicity of polymers used for outdoor insulation", IEEE Trans. Power Delivery, vol. 5, n. 4, pp. 1923-1933, 1990. doi:10.1109/61.103689

[17] Huang, C. M.; Huang, Y. C. "A novel approach to real-time economic emission power dispatch", IEEE Trans. Power Systems, vol. 18, n. 1, 2003, pp. 288-294, doi:10.1109/TPWRS.2002.807071

[18] Kreuger, F. H.; Gulski, E.; Krivda, A. "Classification of partial discharges", IEEE Trans. Electrical Insulation, vol. 28, n. 6, 1993. pp. 917-931. doi:10.1109/14.249365

[19] Ferreira, T. V.; Germano, A. D.; Silva, K. M.; Costa, E. G. “Ultra-sound and Artificial Intelligence Applied to the Diagnosis of Insulations in the Field.” High Voltage Engineering, vol. 38, n. 8, pp. 20061-20066, 2012.

[20] Harrold, R. T. “Acoustic Waveguides for Sensing and Locating Electrical Discharges in High Voltage Power Transformers and other Apparatus.” IEEE Trans. Power Apparatus and Systems, vol. 98, n. 2, pp. 449-457, 1979. doi:10.1109/TPAS.1979.319381

[21] Lundgaard, L. E. “Partial Discharge XIII: acoustic partial discharge detection-fundamental considerations.” IEEE Electrical Insulation Magazine, vol. 8, pp. 25-31, 1992. doi:10.1109/57.145095

[22] Abdel-Salam, M.; Abdel-Sattar, S.; Sayed, Y.; Ghally, M. “Early Detection of Weak Point in MEEC Distribution System.” In: Industry Applications Conf. Record of the 2001 IEEE, 2001, Chicago. vol. 4, pp. 2541–2545. doi:10.1109/IAS.2001.955978

[23] Rocha, P. H. V.; Fontgalland, G. “Measuring the radiation bands of overhead power lines glass insulators”. Proc. of the IEEE 2014 Int. Conf. Antenna Measurements & Applications. France, 2014. doi:10.1109/CAMA.2014.7003395

[24] Dawson, G. A.; Richards, C. N.; Krider, E. P.; Uman, M. A. “The Acoustic Output of a Long Spark”. Journal of Geophysical Research, vol. 73, pp. 815-816, 1968. doi:10.1029/JB073i002p00815

[25] Harrold, R. T. “Acoustical Technology Applications in Electrical Insulation and Dielectrics.” IEEE Trans. Electrical Insulation, vol. 20, n. 1, pp. 3-19, 1985. doi:10.1109/TEI.1985.348751

[26] Gajić, B.; Paliwal, K. K. “Speech Parametrization for Automatic Speech Recognition in Noisy Conditions,” in: Proc. Norwegian Symp. Signal Processing, Trondheim, 2001.

[27] Paliwal, K. K. “Spectral Subband Centroid Features for Speech Recognition,” in: Int. Conf. Acoustics, Speech and Signal Processing, Seattle, vol. 2, pp. 617-620, 1998. doi:10.1109/ICASSP.1998.675340

[28] McCulloch, W. S.; Pitts, W. “A Logical Calculus of the Ideas Immanent in Nervous Activity.” Bulletin of Mathematical Biophysics, vol. 5, pp. 115-133, 1943. doi:10.1007/BF02478259

[29] Haykin, S. O. Neural Networks and Learning Machines. 3. ed. New Jersey: Pearson Prentice Hall, 2008.

[30] Rosenblatt, F. “The Perceptron: A probabilistic model for information storage and organization in the brain,” Psychological Review, vol. 65, pp. 386-408. doi:10.1037/h0042519

[31] Riedmiller, M.; Braun, H. “RPROP - A Fast Adaptive Learning Algorithm”, In: Int. Symp. Computer and Information Science, 1993. doi:10.1109/ICNN.1993.298623

[32] Hagan, M. T; Menhaj, M. B. “Training Feedforward Networks with the Marquardt Algorithm,” IEEE Trans. Neural Networks, vol. 5, pp. 989-993, 1994. doi:10.1109/72.329697

[33] Bishop, C. M. Neural Networks for Pattern Recognition. Clarendon Press, Oxford. 1995.

[34] Kalman, B. L.; Kwasny, S. C. “Why tanh: choosing a sigmoidal function.” In: Int. Joint Conf. Neural Networks, 1992, Baltimore. vol. 2, pp. 578 - 581. doi:10.1109/IJCNN.1992.2272578